Nanoscale

RSC Publishing

PAPER

View Article Online
View Journal | View Issue

Enhancing molecule fluorescence with asymmetrical plasmonic antennas†

Cite this: *Nanoscale*, 2013, **5**, 6545

Guowei Lu,*[a] Jie Liu,[a] Tianyue Zhang,[a] Hongming Shen,[a] Pascal Perriat,[b] Matteo Martini,[c] Olivier Tillement,[c] Ying Gu,[a] Yingbo He,[a] Yuwei Wang[a] and Qihuang Gong*[a]

Received 16th March 2013
Accepted 13th May 2013

DOI: 10.1039/c3nr01306e

www.rsc.org/nanoscale

We propose and justify by the finite-difference time-domain method an efficient strategy to enhance the spontaneous emission of a fluorophore with a multi-resonance plasmonic antenna. The custom-designed asymmetrical antenna consists of two plasmonic nanoparticles with different sizes and is able to couple efficiently to free space light through multiple localized surface plasmon resonances. This design simultaneously permits a large near-field excitation near the antenna as well as a high quantum efficiency, which results in an unusual and significant enhancement of the fluorescence of a single emitter. Such an asymmetrical antenna presents intrinsic advantages over single particle or dimer based antennas made using two identical nanostructures. This promising concept can be exploited in the large domain of light–matter interaction processes involving multiple frequencies.

Introduction

In the past decade, optical nanoantennas based on plasmon nanostructures have emerged as powerful tools to tailor the fluorescence behaviors of molecules and quantum dots.[1,2] Metal surface enhanced effects can improve the detection limit by enhancing the fluorescence intensity greatly, furthermore, the emission direction of molecular fluorescence can also be controlled by such optical antennas.[2,3] Interestingly, plasmonic antennas can change not only the intensity but also the spectral shape of the molecular fluorescence, because the local nanocavity plasmons are able to affect the radiative channels of molecular emitters.[4,5] They, indeed, induce the creation of high local fields associated with localized surface plasmon resonances that can be employed either to maximize the localized excitation field to enhance the fluorescence intensity directly or to increase the radiative decay rate of the emitter through the Purcell effect to engineer the emission process.[6] In this context, to obtain higher fluorescence intensity, the researchers have been increasingly aware of the advantage that would consist of optimizing simultaneously both quantities related to excitation and emission processes through the design of the embedding environment.[7–17]

Such an optimization can be realized *via* the overlap of the localized surface plasmon resonance mode (LSPR) of a plasmonic nanoparticle with, respectively, the absorption and emission bands of the emitter. However, plasmonic systems usually present a limited resonance bandwidth while the molecular fluorescence is generally characterized by a large Stokes' shift. Then, the LSPR mode is very unlikely to cover efficiently both the emitter's absorption and emission bands, which results in a lower enhancement effect than expected. Hence, it is strongly desired to design judiciously the plasmonic nanostructure to confer it multiple LSPR modes able to simultaneously enhance the absorption capability and the emission rate of the fluorophores. Double-resonant optical antennas based on two arms of different lengths, the arms with different materials, even nanoparticles with complex structures have been recently proposed and investigated, thus introducing the concept of multiresonant optical antennas.[18–20] Such asymmetrical antennas with multiresonant LSPR modes to enhance molecular fluorescence have seldom been reported so far.

In this study, we numerically study the emission modifications undergone by an emitter dipole placed in the close vicinity of a multifrequency plasmonic antenna consisting of two gold nanorods with different size. This asymmetrical antenna is expected to couple efficiently with free space light through multiple localized surface plasmon resonances, permitting a strategy to provide, at the same time, a substantial near-field

[a]*Department of Physics and State Key Laboratory for Mesoscopic Physics, Peking University, Beijing 100871, China. E-mail: guowei.lu@pku.edu.cn; qhgong@pku.edu.cn*

[b]*MATEIS, UMR 5510 CNRS, INSA-Lyon, Université de Lyon, 20 av. Albert Einstein, 69621 Villeurbanne Cedex, France*

[c]*LPCML, Université de Lyon, Université Claude Bernard, 43 Bd du 11 novembre 1918, 69622 Villeurbanne Cedex, France*

† Electronic supplementary information (ESI) available: The performance of plasmonic enhanced one-photon fluorescence within the nanogap of symmetrical optical antennas, *i.e.* Rods-L45-L45 and Rods-L60-L60 are formed by end to end coupling the Rod-L45 and Rod-L60 antennas separately; and the performance of plasmonic enhanced two-photon fluorescence by coupling the Rods-L50-L50 and Rods-L70-L70 antennas for comparison. See DOI: 10.1039/c3nr01306e

enhancement of the excitation and a significant increase in the radiative decay rate for a high quantum yield efficiency. Such an asymmetrical antenna provides an efficient strategy to enhance the one- or two-photon fluorescence of an emitter.

Methods

The paper starts by describing the system using finite-difference time-domain (FDTD) calculations in cylindrical coordinates.[21,22] When the emitter orientated in the z direction is placed along the longitudinal axis of the nanorods, the electromagnetic problem can be reduced into two dimensions. The emission of a single point dipole source was referred to as a single fluorescence molecule. The optical antenna efficiency is the ratio of P_{rad}, represents the energy that reaches the far field, to P_{tot} the total power dissipated by the emitter, *i.e.* $\eta_a = \Gamma_{rad}/\Gamma_{tot} = P_{rad}/P_{tot}$. P_{rad} was obtained by integrating the Poynting vector over closed surfaces that contain the nanoantenna and dipolar source, while P_{tot} was obtained over closed surfaces containing the dipolar source only.[22,23] Γ_{rad} (also called the Purcell factor F here) was normalized to the unperturbed rate Γ^0_{rad} of the emitter in the absence of nanostructures. Then, the fluorescence enhancement (S/S_0 where S and S_0 are the emission intensities in the presence and in the absence of the antenna) depends on the Purcell factor F and on the antenna efficiency η_a as follow:

$$\frac{S_f}{S_{f0}} = \frac{\eta_a |p\cdot E|^2}{\eta_0 |p\cdot E_0|^2} \sim F \frac{1}{(1-\eta_0)/F + \eta_0/\eta_a} \quad (1)$$

where p is the transition electric dipole moment and E is the electric field at the emitter position. Due to reciprocity theorem, the electric field enhancement $|p\cdot E|^2/|p\cdot E_0|^2$ can be replaced with the Purcell factor F.[23,24] And because of the high value of the Purcell factor F in our system, the fluorescence enhancement can be written as the relation $S/S_0 \propto F_{(\omega)}\cdot\eta_{a(\omega)}$, when the original quantum efficiency of the emitter is assumed as unit in the absence of the antenna. Different key issues will be examined among which the exact contribution of each mechanism in the whole fluorescence process and the influence of some parameters such as the emitter–antenna separation on the near-field enhancement effects. Three dimensional (3D) FDTD calculations will be finally applied to investigate the localized surface plasmon resonance modes of the system through the determination of the near-field light distribution and that of the extinction spectrum. Finally, we will demonstrate that such an asymmetrical antenna can be further implemented efficiently in the field of plasmonic enhanced two-photon fluorescence. In all calculations, the emitter and the antenna are embedded within a homogeneous medium with a refractive index $n = 1.33$ equal to that of water. The optical dielectric function of the gold material is modeled with a Drude–Lorentz dispersion model.[25,26]

Results and discussion

A consensus in the field of plasmonic enhanced spontaneous emission establishes that an elongated particle can more strongly increase the radiative decay rate while maintaining high quantum efficiency in the near-infrared regime than a nanosphere with the same volume.[7,10–13,22] This is mainly due to the imaginary part of the dielectric function that is smaller in the near-infrared region and to the enhancement of the excitation field expected to be strong at the apex of the elongated particle. Furthermore, the emission of a dipole can be enhanced significantly more by placing it within the gap of two metallic nanoparticles than in front of a single one. On the basis of theoretical and experimental studies, two particles with identical geometry are considered to couple together to form an efficient dimer antenna.[14–16] In what follows, we will show that asymmetrical antennas consisting of two different particles with specific properties can provide a more efficient way to enhance the spontaneous emission of fluorescence molecules.[27–34]

Let us begin by examining a typical system of an emitter coupled to a single gold nanorod (*i.e.* an elongated particle) with different separations; the emitter orientation was fixed along the longitudinal axis of the antenna. The solid lines in Fig. 1 represent the wavelength dependence of the optical antenna efficiency η_a. The dashed curves show the wavelength dependence of Γ_{rad}, *i.e.* F for different emitter–antenna separations (*e.g.* 2 nm, 5 nm, 10 nm, and 15 nm, respectively). Additionally,

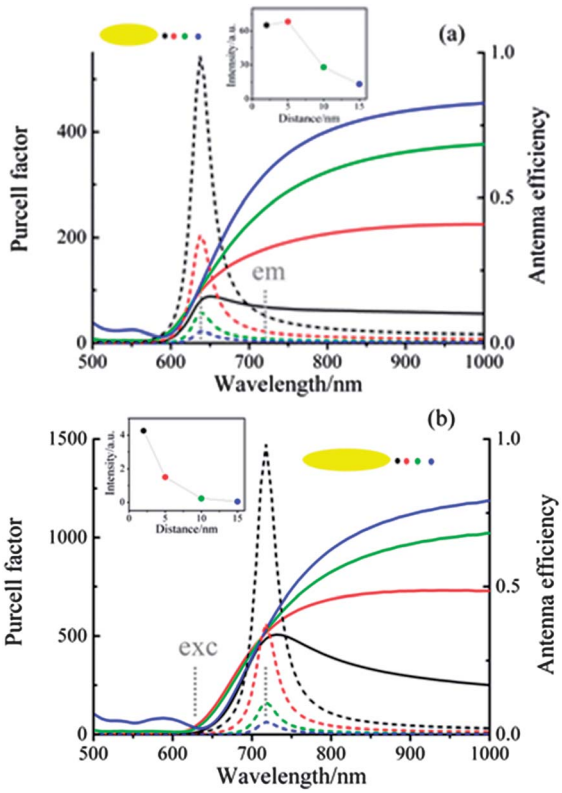

Fig. 1 Wavelength evolution of antenna efficiency η_a (solid lines) and Purcell factor F (dashed lines). The emitter is coupled either to the single gold nanorod Rod-L45 (a) or to the Rod-L60 (b) with different emitter–antenna separations of 2 nm, 5 nm, 10 nm and 15 nm. The inset shows the corresponding relative fluorescence intensities, *i.e.* $S/S_0 \propto F_{(\omega)}\cdot\eta_{a(\omega)}$, for these different distances. The grey straight lines indicate the wavelength of excitation (~630 nm) and that of emission (~730 nm) respectively.

the dotted data in the inset of Fig. 1 display the fluorescence enhancements calculated for different emitter–antenna distances when the excitation and emission present the large Stokes' shift indicated by the grey dashed lines. In such a typical system, it is obvious that, due to its limited width, the longitudinal LSPR peak of the nanorods can be only tuned to overlay either the excitation source or the emission peak of the fluorescent molecules.

The fluorescence enhancement is often explained on the basis of a two-step process: (1) an enhancement of the excitation (or absorption) in the local environment modulated by the plasmonic nanostructures, and (2) a perturbation of the emission rate leading to a new balance between radiative and non-radiative decays depending on the emitter–antenna interaction. For the short nanorod termed Rod-L45 (with a diameter of 20 nm and a length of 45 nm), the emitter excitation ($\lambda \sim$ 630 nm) lies in the LSPR band. This results in a large excitation enhancement evidenced by the high values taken by the Purcell factor around this wavelength (Fig. 1(a)). Expectedly, this enhancement is higher for small emitter–particle distances, the electromagnetic field being concentrated in the vicinity of the metal structure. However, the antenna quantum efficiency decreases rapidly when the emitter–antenna separation decreases which is explained by the well-known fluorescence quenching effect that predominates at a very close distance. The antenna efficiency is maximal for distances of the order of magnitude of the metal size, certainly due to the addition of a new radiative path proposed first by Lakowicz in the framework of the Radiative Decay Engineering (RDE) theory.[5] A certain distance between the particle and the emitter is required to avoid any quenching effect and get a detectable increase in the radiative decay rate. The plasmonic-enhanced fluorescence intensity often presents a maximum at certain separation as the molecule–nanoparticle separation varies.[5,10,11,17]

When studying the nanorod Rod-L60 (with a diameter of 20 nm and a length of 60 nm), the LSPR band is now tuned to the fluorescence emission peak at $\lambda \sim$ 730 nm. This permits a noticeable increase in the antenna quantum efficiency (around 0.35 instead of 0.2 for Rod-L45) even for antenna–emitter distances as small as 2 nm.[35–37] However, the Purcell factor, that is also globally augmented, is drastically red-shifted so that the excitation enhancement is now almost completely suppressed. This leads to a strong reduction in the fluorescence intensity in comparison with the shorter nanorod (around 2 instead of 30 in arbitrary units, depending on the emitter–particle separation, see the inset of Fig. 1(b)). All these results illustrate how it is untrivial to design a plasmonic antenna that preserves a high antenna quantum efficiency and, at the same time enhances the excitation for very short antenna–emitter separations. It should been pointed out that, even if in practice LSPR bands sufficiently broad to overlap both excitation and emission bands are often encountered, they are generally caused by unavoidable and damageable fabrication deviations that systematically lead to lower enhancements than expected.[35,38]

Having demonstrated the limit of plasmonic-induced fluorescence enhancement in systems containing only one LSPR mode, we now explore the possibility of enhancing both the excitation and the emission of spontaneous emitters by the use of two coupled elongated particles where the antenna can present multiresonances. The central idea is to design a multifrequency antenna that can directly couple with free space light at, at least, two resonances. This would result in both a strongly concentrated near-field and a high emission efficiency at the same spatial position and with the same polarization direction. Even if nanostructures with complicated shapes (*e.g.* triaxial nanoellipsoids[39]) can be designed to possess multiple plasmon resonances, current and feasible experimental routes permit us to easily obtain the asymmetrical antenna described above. These routes consist of the well controlled nanofabrication techniques that are based on, for example, focusing ion beam etching or electron beam lithography *etc.* These techniques have already been employed to successfully design setups permitting the control of the nonlinear response of certain materials.[29] Then, in a four-wave mixing process, the multifrequency antennas consisting of two arms with different lengths have resonances at two different incoming frequencies resulting in a large output signal centered at a third frequency determined by a nonlinear optical material filling the separation gap. Inspired by this design and by the fact that the emission usually undergoes a larger enhancement within the gap of coupled elongated nanoparticles, we try to extend the concept of multifrequency antenna to the field of plasmonic enhancement of spontaneous fluorophores emission.

Here, an asymmetrical optical antenna is formed by the end to end coupling of both Rod-L45 and Rod-L60 with a gap separation of 20 nm. Fig. 2 and its inset show, for different locations of the emitter within the gap, the wavelength dependence of the antenna efficiency and of the relative radiative rate as well as the value of the fluorescence enhancement. As expected, two distinct LSPR bands are now lying at the excitation and emission centers. The excitation enhancement is maximal when the emitter is placed in the close vicinity of the

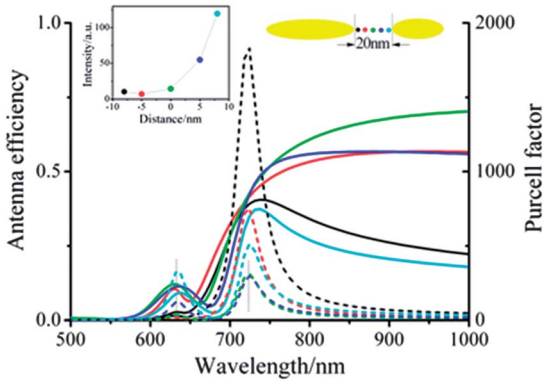

Fig. 2 Wavelength evolution of antenna efficiency η_a (solid lines) and Purcell factor F (dashed lines). An emitter is placed within the gap of an asymmetrical antenna, made by coupling the nanorods Rod-L45 and Rod-L60 for different emitter–antenna separations of 2 nm, 5 nm and 10 nm respectively. The insets show the corresponding relative fluorescence intensities, *i.e.* $S/S_0 \propto F_{(\omega)} \cdot \eta_{a(\omega)}$ for these different distances. As in Fig. 1, the grey straight lines indicate the wavelengths of excitation and emission.

arm possessing the appropriate resonance frequency (Rod-L45 for 630 nm and Rod-L60 for 730 nm). The emitter must then be located near the Rod-L45 to benefit from the more significant enhancement of excitation. Moreover, the antenna quantum efficiency can preserve high values for frequencies around 731 nm. Hence the relative fluorescence enhancement caused by the use of the asymmetrical antenna is obviously larger than that induced by the presence of only one nanorod regardless of its size (see the inset of Fig. 2). It is also larger than that originating from the symmetrical antenna in the case of the antennas with both identical arms, *i.e.* made for the first one by the end to end coupling of two Rod-L45 nanorods and, for the second one, by the coupling of two Rod-L60 nanorods whose calculated performances are given in the ESI.† Obviously the custom-designed asymmetrical antenna with multiple LSPR modes permits a large near-field excitation as well as a high quantum efficiency, which results in a significant enhancement of the molecular fluorescence.

To highlight differently the advantage of multifrequency antennas, we compare in detail the fluorescence performance induced by different antennas characterized by the same short separation of 2 nm from the emitter. The results are summarized in Table 1. Although the single Rod-L45 antenna presents a high excitation enhancement, the related quantum efficiency is low which does not lead to an optimized fluorescence enhancement. Only the asymmetrical antenna Rods-L45-L60 can display a large field enhancement and at the same time maintain a high quantum efficiency, which are the conditions needed to get a strong fluorescence enhancement. Symmetrical coupled antennas such as Rods-L45-L45 or Rods-L60-L60 also possess two resonance bands due to the coupling of the dipolar resonance of both nanorods. These bands are often assigned to bonding and anti-bonding modes respectively.[40,41] However, the anti-bonding modes of the symmetrical antennas are dark modes, that are unlikely to couple to free space light because the dipoles of individual antenna are anti-aligned and cancel each other resulting in no net dipole moment. The incident light wave can only strongly couple to the dipolar bonding mode which leads to just one LSPR mode around the excitation or emission range respectively. In contrast, the antenna Rods-L45-L60 can efficiently couple to free space light at two resonant bands thanks to its asymmetrical configuration. This provides an efficient way to control both the excitation and emission processes simultaneously. Interestingly, a higher spontaneous emission enhancement could be still achieved by shorting the gap between the two particles. This constitutes a further improvement that will not be discussed here in more detail.

To demonstrate even more clearly the performances allowed by the use of asymmetrical antennas, we have computed the extinction spectra and near-field electromagnetic distributions employing the 3D FDTD method. Only the longitudinal plasmon resonances of the antenna were calculated since the electric field polarization of the plane wave was set parallel to the longitudinal axis of the rods. As seen from Fig. 3(a), two resonance bands are then observed peaking, as expected, at the wavelengths of 630 and 730 nm, respectively. This consists of additional proof that, in contrast to symmetrical ones, the asymmetrical antenna can efficiently couple to free space light at several frequencies. Then, the near field distributions were computed at the resonant frequencies for two different irradiations characterized by a continuous plane-wave source at $\lambda \approx 645$ nm or $\lambda \approx 735$ nm, respectively (Fig. 3(b) and (c)). For an excitation light at $\lambda \approx 735$ nm, Fig. 3(c) reveals the presence of an electromagnetic enhancement in the vicinity of both arms. In contrast, for an excitation at 645 nm, the enhancement appears less concentrated around the long arm and attains significant values near the short arm only (Fig. 3(b)). This explains why the extinction values calculated at 735 nm are higher than those at 645 nm (Fig. 3(a)). This also explains why placing the emitter close to

Table 1 Relative contributions of the excitation and quantum yield efficiency to the total fluorescence enhancement of an emitter placed in the vicinity of various nanostructures compared to the free space

Nanostructures	η_{exc}	η_{ant}	η_F
Rod-L45	469	0.12	56
Rod-L60	12	0.34	4.1
Rods-L45-L45	320	0.2	64
Rods-L60-L60	14	0.48	6.7
Rods-L45-L60	324	0.37	120

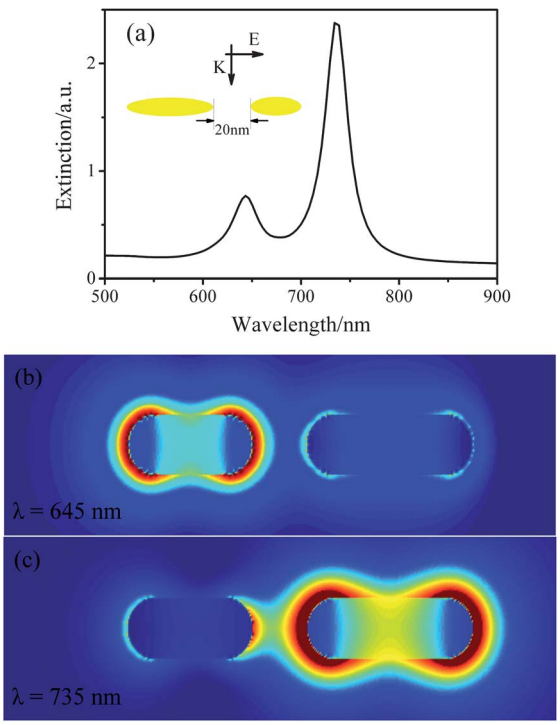

Fig. 3 Calculated and field distribution near the asymmetrical antenna made of two gold nanorods of lengths 45 and 60 nm, respectively. (a) The extinction spectrum of the antenna illuminated by a broadband plane wave parallel to the longitudinal axis. (b and c) The near field distributions in the vicinity of the asymmetrical antenna irradiated by a continuous plane wave at the frequency $\lambda \approx 645$ nm or $\lambda \approx 735$ nm, respectively.

the short arm is required to favor some excitation enhancement at 630 nm. At the emission wavelength of 730 nm, field enhancement is weak near the short arm in the absence of the other rod (data not shown). This is related to the low efficacy of the single Rod-L45 considered as an antenna. In contrast, in the presence of the Rod-L60, a certain enhancement, a little less significant but still comparable to that near the long arm, is observed at 730 nm. Using the reciprocity theorem, we argue that the emission of a spontaneous emitter can undergo a large enhancement within the gap of an asymmetrical antenna even if the emitter is placed near the short arm. The long arm possessing a resonant mode at the emission band helps to extract light emission to free space. Consequently, the quantum efficiency near the short arm of an asymmetrical antenna is obviously greater than that observed in the vicinity of a single rod.

In a similar way, such an asymmetrical antenna can be used efficiently in the field of plasmonic enhanced two-photon fluorescence (TPF). TPF is growing in popularity because of its highly confined excitation, intrinsic three dimensionality of images, and reduced photodamage.[42] In recent years many efforts have been made to improve the performance of TPF and metal-enhanced TPF has now become an appealing scheme based on the interactions between fluorophores and plasmonic nanoparticles. However, to optimally enhance the TPF intensity, it should be also desirable that the plasmonic spectral features overlap both fluorophores' absorption and emission simultaneously. We already proposed to achieve such an enhancement *via* the dipolar and quadrupolar modes of a single plasmonic nanostructure.[43] The dipolar resonance coupled with the incident light resulting in a large localized field enhancement. At the same time, the radiative quadrupolar mode overlapped the emission band of the excited fluorophores to assist the fluorescence emission. However, the LSPR tailoring of the asymmetrical antenna presenting two resonance peaks is experimentally more feasible than that of single plasmonic nanostructures with dipolar and quadrupolar modes. We therefore demonstrate in this paper that the concept of multi-frequency antennas designed for the plasmonic enhancement of one-photon fluorescence emission can also be extended to the TPF process.

Here, the TPF signal S of an isolated emitter is: $S \propto k \cdot \sigma^{2P}_{(\omega)} \cdot \eta_{(\omega)} \cdot |p \cdot E|^4$. In this relation, k is the collection efficiency (assumed to remain the same in the absence or in the presence of the nanostructure), $\sigma^{2P}_{(\omega)}$ is the two-photon absorption cross-section of the fluorophores, $\eta_{(\omega)}$ is the quantum efficiency of the emitter, p is the transition electric dipole moment and E is the electric field at the emitter position. It should be noted that we mainly consider how the metallic nanostructures modify the excitation and emission rates during the metal-enhanced TPF as the conventional way in the metal-enhanced one-photon excitation fluorescence. Whereas the process of the plasmonic enhanced TPF should be more complex in practice. For simplicity, the TPF brightness of the emitter is approximately only related to the local field enhancement and the quantum efficiency due to the influencing of the plasmonic antenna. The single Rod-L50 (with a diameter of 20 nm and a length of 50 nm) and Rod-L72 (with a diameter of 20 nm and a length of 72 nm) were chosen to demonstrate the plasmonic enhancement in the case of TPF since their resonances peak at $\lambda \approx 663$ nm and $\lambda \approx 785$ nm, respectively. These peaks lie in a wavelength range that corresponds to, on one hand, the emission band of the widely used Cy5 fluorophore molecule and, on the other hand, to the pulsed excitations delivered by the lasers generally used for two-photon fluorescence. As demonstrated above, the dipolar mode of a single nanorod can only overlay the emission or excitation which results in an enhancement of only one of the processes involved in TPF, *i.e.* either excitation (absorption) or emission (quantum yield). To illustrate this, the antenna efficiency and the Purcell factor of a single nanorod calculated in the case of a TPF configuration are shown in the ESI (Fig. S2†). We also compare the plasmonic enhanced TPF performance induced by different antennas (symmetric and asymmetric) placed at the same short separation of 2 nm from the emitter (Table 2). The main conclusions are similar to those developed in the case of the one-photon fluorescence process. As expected, the optimized plasmonic enhancement of TPF is obtained with the coupled nanorods Rods-L72-L50 (see Fig. 4 that details the results).

Table 2 Relative contributions of the excitation and quantum yield efficiency to the total two-photon fluorescence enhancement of an emitter placed in the vicinity of various nanostructures by comparison with those obtained in free space

Nanostructures	η_{exc}	η_{ant}	η_F
Rod-L50	43	0.19	356
Rod-L72	2040	0.009	37 300
Rods-L50-L50	94	0.18	1630
Rods-L72-L72	750	0.014	7830
Rods-L72-L50	2500	0.06	376 800

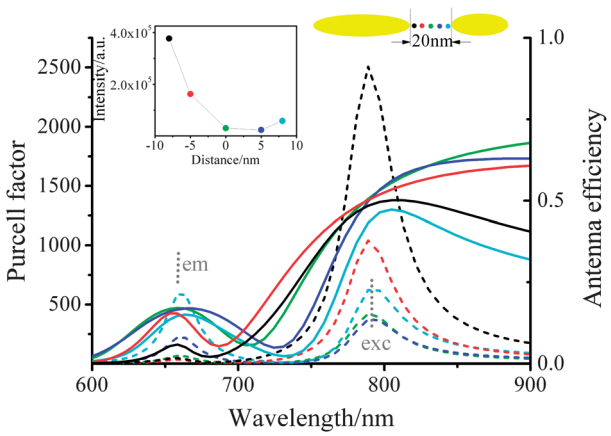

Fig. 4 Wavelength evolution of antenna efficiency η_a (solid lines) and Purcell factor F (dashed lines) in a TPF process. An emitter is placed within the gap of an asymmetrical antenna, made by coupling the nanorods Rod-L50 and Rod-L72 for different emitter–antenna separations of 2 nm, 5 nm and 10 nm respectively. The insets show the corresponding relative TPF signal for these different distances. As in Fig. 1, the grey straight lines indicate the wavelengths of excitation and emission.

Conclusions

In summary, we have presented and justify by employing FDTD calculations an efficient strategy to enhance the one- or two-photon fluorescence of an emitter with a multifrequency asymmetrical antenna. Such an asymmetrical antenna is able to couple efficiently to free space light through multiple localized surface plasmon resonances. The near-field enhancement near the antenna is large, and at the same time the system maintains a high quantum efficiency, which permits the spontaneous emission to be significantly enhanced. This concept can be exploited in the large domain of the light–matter interaction research by the careful fabrication of systems containing, at the same time, different antenna and emitters. In particular, asymmetrical antenna appear as promising tools to modulate, *via* multi-plasmonic resonant modes, the input and output signals in advanced set-ups based on, for example, non-linear processes of four-wave mixing or coherent anti-stokes Raman scattering phenomena.

Acknowledgements

This work was supported by the National Key Basic Research Program of China (grant no. 2013CB328703 and 2009CB930504) and the National Natural Science Foundation of China (grant no. 61008026, 11121091, 90921008).

Notes and references

1 K. T. Shimizu, W. K. Woo, B. R. Fisher, H. J. Eisler and M. G. Bawendi, *Phys. Rev. Lett.*, 2002, **89**, 117401.
2 H. Aouani, O. Mahboub, N. Bonod, E. Devaux, E. Popov, H. Rigneault, T. W. Ebbesen and J. Wenger, *Nano Lett.*, 2011, **11**, 637–644.
3 T. H. Taminiau, F. D. Stefani, F. B. Segerink and N. F. Van Hulst, *Nat. Photonics*, 2008, **2**, 234–237.
4 M. Ringler, A. Schwemer, M. Wunderlich, A. Nichtl, K. Kürzinger, T. A. Klar and J. Feldmann, *Phys. Rev. Lett.*, 2008, **100**, 203002.
5 Z. C. Dong, X. L. Zhang, H. Y. Gao, Y. Luo, C. Zhang, L. G. Chen, R. Zhang, X. Tao, Y. Zhang, J. L. Yang and J. G. Hou, *Nat. Photonics*, 2010, **4**, 50–54.
6 E. M. Purcell, *Phys. Rev.*, 1946, **69**, 681.
7 J. R. Lakowicz, *Anal. Biochem.*, 2005, **337**, 171–194.
8 E. Fort and S. Gresillon, *J. Phys. D: Appl. Phys.*, 2008, **41**, 013001.
9 P. Biagioni, J. S. Huang and B. Hecht, *Rep. Prog. Phys.*, 2012, **75**, 024402.
10 P. Anger, P. Bharadwaj and L. Novotny, *Phys. Rev. Lett.*, 2006, **96**, 113002.
11 T. Hartling, P. Reichenbach and L. M. Eng, *Opt. Express*, 2007, **15**, 12806–12817.
12 A. Moroz, *Chem. Phys.*, 2005, **317**, 1–15.
13 L. Rogobete, F. Kaminski, M. Agio and V. Sandoghdar, *Opt. Lett.*, 2007, **32**, 1632–1635.
14 A. Kinkhabwala, Z. Yu, S. Fan, Y. Avlasevich, K. Mullen and W. E. Moerner, *Nat. Photonics*, 2009, **3**, 654–657.
15 O. L. Muskens, V. Giannini, J. A. Sanchez-Gil and J. Gomez Rivas, *Nano Lett.*, 2007, **7**, 2871–2875.
16 A. Bek, R. Jansen, M. Ringler, S. Mayilo, T. A. Klar and J. Feldmann, *Nano Lett.*, 2008, **8**, 485–490.
17 G. Lu, H. Shen, B. Cheng, Z. Chen, C. A. Marquette, L. J. Blum, O. Tillement, S. Roux, G. Ledoux, M. Ou and P. Perriat, *Appl. Phys. Lett.*, 2006, **89**, 223128.
18 K. Thyagarajan, S. Rivier, A. Lovera and O. J. F. Martin, *Opt. Express*, 2012, **20**, 12860–12865.
19 T. Shegai, S. Chen, V. D. Miljković, G. Zengin, P. Johansson and M. Käll, *Nat. Commun.*, 2011, **2**, 481–486.
20 F. Hao, C. L. Nehl, J. H. Hafner and P. Nordlander, *Nano Lett.*, 2007, **7**, 729–732.
21 A. F. Oskooi, D. Roundy, M. Ibanescu, P. Bermel, J. D. Joannopoulos and S. G. Johnson, *Comput. Phys. Commun.*, 2010, **181**, 687–702.
22 G. Lu, T. Zhang, W. Li, L. Hou, J. Liu and Q. Gong, *J. Phys. Chem. C*, 2011, **115**, 15822–15828.
23 A. Mohammadi, F. Kaminski, V. Sandoghdar and M. Agio, *J. Phys. Chem. C*, 2010, **114**, 7372–7377.
24 T. H. Taminiau, F. D. Stefani and N. F. van Hulst, *New J. Phys.*, 2008, **10**, 105005.
25 A. Vial, A.-S. Grimault, D. Macias, D. Barchiesi and M. L. de la Chapelle, *Phys. Rev. B: Condens. Matter Mater. Phys.*, 2005, **71**, 085416.
26 P. B. Johnson and R. W. Christy, *Phys. Rev. B: Solid State*, 1972, **6**, 4370–4379.
27 M. P. Busson, B. Rolly, B. Stout, N. Bonod and S. Bidault, *Nat. Commun.*, 2012, **3**, 962.
28 J. Liaw, J. Chen, C. Chen and M. Kuo, *Opt. Express*, 2009, **16**, 13532–13540.
29 H. Harutyunyan, G. Volpe, R. Quidant and L. Novotny, *Phys. Rev. Lett.*, 2012, **108**, 217403.
30 H. Aouani, M. Navarro-Cia, M. Rahmani, T. P. H. Sidiropoulos, M. Hong, R. F. Oulton and S. A. Maier, *Nano Lett.*, 2012, **12**, 4997–5002.
31 M. Abb, Y. Wang, P. Albella, C. H. de Groot, J. Aizpurua and O. L. Muskens, *ACS Nano*, 2012, **6**, 6462–6470.
32 L. Shao, C. H. Fang, H. J. Chen, Y. C. Man, J. F. Wang and H.-Q. Lin, *Nano Lett.*, 2012, **12**, 1424–1430.
33 N. A. Cinel, S. Butun, G. Erta and E. Ozbay, *Small*, 2013, **9**, 531–539.
34 L. S. Slaughter, Y. Wu, B. A. Willingham, P. Nordlander and S. Link, *ACS Nano*, 2010, **4**, 4657–4666.
35 S. Gerber, F. Reil, U. Hohenester, T. Schlagenhaufen, J. R. Krenn and A. Leitner, *Phys. Rev. B: Condens. Matter Mater. Phys.*, 2007, **75**, 073404.
36 F. Tam, G. P. Goodrich, B. R. Johnson and N. J. Halas, *Nano Lett.*, 2007, **7**, 469–477.
37 Y. Chen, K. Munechika and D. S. Ginger, *Nano Lett.*, 2007, **7**, 690–696.
38 P. P. Pompa, L. Martiradonna, A. Della Torre, F. Della Sala, L. Manna, M. De Vittorio, F. Calabi, R. Cingolani and R. Rinaldi, *Nat. Nanotechnol.*, 2006, **1**, 126–130.
39 D. V. Guzatov and V. V. Klimov, *Chem. Phys. Lett.*, 2005, **412**, 341–350.

40 P. Nordlander, C. Oubre, E. Prodan, K. Li and M. I. Stockman, *Nano Lett.*, 2004, **4**, 899–903.
41 Z. J. Yang, Z. S. Zhang, W. Zhang, Z. H. Hao and Q. Q. Wang, *Appl. Phys. Lett.*, 2010, **96**, 131113.
42 P. T. C. So, C. Y. Dong, B. R. Masters and K. M. Berland, *Annu. Rev. Biomed. Eng.*, 2000, **2**, 399–429.
43 T. Zhang, G. Lu, J. Liu, H. Shen, P. Perriat, M. Martini, O. Tillement and Q. Gong, *Appl. Phys. Lett.*, 2012, **101**, 051109.